Applied Radiation and Isotopes 214 (2024) 111548

Contents lists available at ScienceDirect

Applied Radiation and Isotopes

journal homepage: www.elsevier.com/locate/apradiso

Structural, vibrational, and luminescent properties of pure and Ce-doped magnesium lithium aluminoborate glass

Allan W.S. Santos [a], Iury S. Silveira [b], Luiz C. Meira-Belo [c], Andrea L.F. Novais [d], Divanizia N. Souza [a,*]

[a] Departamento de Física, Universidade Federal de Sergipe, São Cristóvão, SE, Brazil
[b] Instituto de Pesquisas Energéticas e Nucleares, IPEN/CNEN, São Paulo, SP, Brazil
[c] Centro de Desenvolvimento da Tecnologia Nuclear, CDTN/CNEN, Belo Horizonte, MG, Brazil
[d] Faculdade de Engenharia Mecânica, Universidade Federal Do Sul e Sudeste Do Pará, Marabá, Pará, Brazil

A B S T R A C T

The objective of this work was to study the properties of new vitreous samples of pure BAlMgLi and Ce-doped BAlMgLi produced by the melt-quenching method. The structural and vibrational characteristics of the samples were analyzed using x-ray diffraction (XRD), vibrational Raman spectroscopy, and vibrational Fourier transform infrared spectroscopy (FTIR). Optically stimulated luminescence (OSL) and thermoluminescence (TL) techniques were also used to identify whether the samples showed a response to ionizing radiation. XRD analyses confirmed the predominance of the amorphous phase of the samples. The Raman spectra revealed that the atomic bonds present in the material matrix are of the pyroborate and metaborate type, enabling stretching vibrations in isolated BO_4 and/or Al–O or Al–O–B units. The band at approximately 810 cm^{-1} is characteristic of the formation of the boroxol ring, indicating that the presence of other elements in the matrix does not affect its glassy characteristics. The FTIR analyses reinforce the results found by Raman spectroscopy, because bands characteristic of low hygroscopic glasses were observed, due to the conversion of BO_3 units into BO_4 in triborate, tetraborate, and pentaborate groups. This conversion is due to dopant entrainment, which contributes to the high optical transparency of the samples. Their OSL and TL signals were reproducible with intensities dependent on the dopant concentration and radiation dose, with the most intense emissions resulting from 0.5% Ce concentrations.

1. Introduction

Glass materials are considered a subgroup of ceramic materials and are currently the focus of studies for application in personal dosimetry as passive-type detectors (Del Sol Fernández et al. (2016); Rivera-Montalvo et al. (2021); López-Esquivel et al. (2023); Ugalde-Valdés et al. (2023); León-Alfaro et al., 2018). Presently, glasses have been widely studied for dosimetric applications because they have intrinsic properties of great relevance, such as ease of production, large-scale reproducibility with low production cost, easy handling, and flexible chemical compositions. This makes it easy to incorporate different elements into the structure, allowing the achievement of complex structural matrices (Yahaba et al., 2017). These materials have a diversity of properties that can accrue from different structural combinations, favoring the emergence of mechanical, optical, thermal, physical, and chemical properties or in the improvement of these properties (Feller et al., 1997).

The luminescent materials most employed in clinical and personal dosimetry have low effective atomic numbers (Z_{eff}), similar to soft tissue, which is a relevant property from the point of view of bioequivalence because the interaction processes of ionizing radiation depend on the Z_{eff} of the material (Bos, 2001). The luminescent characteristics of a material are mainly defined by its sensitivity to the radiation dose, linearity between the radiation dose and the respective luminescent response, and by fading of its luminescent signal, which should be relatively low (Nakauchi et al., 2017; Omar et al., 2022).

Compounds containing boron as the main network former, borates, have been the target of several studies, especially with glass formation for dosimetric applications, such as strontium tetraborate (SrB_4O_7), which has sensitivity equivalent to the commercial thermoluminescent dosimeter TLD-700, and $Li_2B_4O_7$ doped with copper, which has TL sensitivity almost eight times higher than the TLD-100. Strontium and calcium, as network modifiers in the borate matrix, have been incorporated into borate-based glass matrices studied for use as a radiation detector (Huang et al., 2022; Sadeq and Abdo, 2021; Mohan et al., 2017; Kawano et al., 2018; Dogan et al., 2017; Santiago et al., 1998; Alajerami et al., 2013).

Borate glasses present a low melting point, high rare-earth element accommodation capacity, and a Z_{eff} close to that of human tissue

* Corresponding author.
E-mail address: divanizia@gmail.com (D.N. Souza).

https://doi.org/10.1016/j.apradiso.2024.111548
Received 26 February 2024; Received in revised form 16 August 2024; Accepted 7 October 2024
Available online 10 October 2024

(approximately 7.35), which is a useful feature in personal radiation monitoring, and low production cost (Kawano et al., 2018; Rittisut et al., 2022). Borates combined with Al_2O_3 and other elements such as magnesium, lithium, and cerium can result in transparent glasses with high radiation sensitivity and linearity between the luminescent response and the absorbed dose (Vogel, 1994; Souza et al., 2021; Elkholy, 2010). The transparency of a material of dosimetric interest is a desirable characteristic when its luminescence must be collected efficiently (Bos, 2001; Hashim et al., 2014; Barrera et al., 2019). In more recent studies by Nakauchi et al. (2017), magnesium was introduced into the B_2O_3 matrix, conferring better luminescent properties, with Zeff values even closer to that of human tissue. In the other hand, lithium contributes to an increase in the viscosity of the melt and a decrease in the melting temperature (El-Adawy et al., 2010; Elkholy, 2010; Alajerami et al., 2013).

The physical and chemical properties of the glass contribute to the incorporation of optically active ions with a wide range of optical transmission, chemical, thermal stability and in radiation dosimetry (Daisuke et al., 2017; Zubair et al., 2020; Kaur et al., 2021). Therefore, studies on the applicability of glasses in ionizing radiation dosimetry using luminescence techniques such as optically stimulated luminescence (OSL), thermoluminescence (TL), and radiophotoluminescence (RPL) have been enthusiastically carried out in recent times (Barrera et al., 2019; Kitagawa et al., 2021; Li et al., 2024).

The use of rare earths has been widely explored in glass matrix studies. These elements are transition metals belonging to the lanthanide family, they have incompletely filled or unfilled orbitals in the 4f and 5 d layers. Cerium is normally used in glasses in its Ce^{3+} oxidation state, thus exhibiting high optical absorption and fluorescence in the near ultraviolet (UV) region and in the visible and mid-infrared and 4f electronic configuration, with transitions between electronic configuration states allowed 4f and 5 d (Kaur et al., 2013). The energy difference between these levels being very wide, not allowing non-radioactive decay (Daisuke et al., 2017). Due to its luminescence enhancing properties, Ce^{3+} has been used as a dopant in materials of interest for TL and OSL dosimetry (Kucuk et al., 2016; Oglakci et al., 2020, 2023).

In this work, new vitreous samples of pure BAlMgLi and Ce-doped BAlMgLi, whose Z_{eff} is 11.46, were produced, and their structural, vibrational, and luminescent properties were studied. In the case of luminescent analyses, the interest was to identify whether the samples have potential for use in ionizing radiation dosimetry. Samples were prepared using the melt-quenching synthesis method, which is widely used for a rapid preparation of glass composites with metastable phases (Vogel, 1994; Iordanova et al., 2009). This method is simple, inexpensive, and produces glass samples of high homogeneity. The preparation of the glass samples basically consists of mixing the reagents in a stoichiometric manner and heating them in an oven at high temperatures, on the order of 900 °C–1400 °C. (Ardiansyah et al., 2023).

2. Material and methods

The reagents used in the preparation of the vitreous samples and the corresponding percentages of reagent purity were as follows: boric acid – H_3BO_3 (99.5%), aluminum -Al_2O_3 (99.5%), magnesium oxide – MgO (95.0%), lithium carbonate – Li_2CO_3 (98.0%), and cerium oxide - CeO_2 (99.9%). Each sample was prepared in three steps. In the first step, the reagents were mixed stoichiometrically in an agate mortar and heated at a rate of 10 °C/min from room temperature to 600 °C in an open furnace atmosphere, where mixture was held for 4 h to decarbonate the lithium. In the second step, the mixture was heated to 1150 °C at a rate of 30 °C/min and held at this temperature for 1 h to allow the reagents to melt homogeneously. Finally, the sample was poured into an aluminum mold (at 300 °C) where it remained for 1 h to relieve structural stress and avoid possible cracks caused by sudden temperature changes.

For structural and vibrational analysis, the glass samples were crushed and sieved (75 μm–150 μm). The powder obtained was used for analysis by X-ray diffraction (XRD), Raman and Fourier transform infrared (FTIR). For infrared spectroscopy, the powder was mixed with KBr, which is used as a support in this technique and allows accurate measurements without blocking the light path. Finally, the glasses were pressed and sintered at 300 °C for luminescent studies. The analyses were performed at an ambient temperature of 22 °C. Raman, FTIR, and infrared spectroscopy estimates are the results of the weighted average of a total of ten consecutive measurements.

The glassy structure of the samples was confirmed by XRD analyses performed in a PANalytical diffractometer with a linear detector (Xcelerator) in the Bragg-Breton θ–2θ configuration. The radiation used in the equipment was the Cu Kα ($\lambda = 1.5444$ Å). The diffractograms were obtained with a step of 0.026° per minute in an acquisition time of 1 s, in the range from 10° to 80°.

Raman spectroscopy was performed with a Senterra dispersive Raman spectrometer manufactured by Bruker Optik GmbH. Analyzes were performed with the instrument configured on a 633 nm He-Ne laser with an intensity of 10 mW and an integration time of 100 s. The objective aperture was 2 mm and the resolution was 3–5 cm^{-1} in the region of 200–3500 cm^{-1}, keeping the samples isolated from ambient light. The baseline was taken into account to ensure the reliability of the measurements.

FTIR vibrational spectroscopy measurements were performed on a PerkinElmer Spectrum Two FTIR in an open atmosphere, with a measuring range between 0 and 4000 cm^{-1}.

The optically stimulated luminescent (OSL) and thermoluminescent (TL) data were obtained from a Riso TL/OSL reader, Model DA-20. A Hoya U 340 filter with peak transmission (~90%) at 340 nm and window centered at ~365 nm was used in the TL/OSL reader. The beta radiation source ($^{90}Sr + {}^{90}Y$) had a dose rate of 81.6 mGy s^{-1}. For the OSL signal measurement, continuous blue LED stimulation was applied for 40 s, with peak emission at 470 nm. For TL, the samples were heated from 25 to 325 °C with a heating rate of 5 °C s^{-1} under nitrogen flow. Each luminescence measurement process was repeated for three samples under the same conditions. The maximum uncertainty of the measurements was ±9%.

The optically stimulated luminescence (OSL) and thermoluminescence (TL) data were obtained from a Riso TL/OSL reader, Model DA-20. A Hoya U 340 filter with peak transmission (~90%) at 340 nm and window centered at ~365 nm was used in the TL/OSL reader. Samples are 6 mm in diameter and 1 mm thick. The beta radiation source ($^{90}Sr + {}^{90}Y$) presented a dose rate of 81.6 mGy s^{-1}. To measure the OSL signal, continuous blue LED stimulation was applied for 40 s, with an emission peak at 470 nm. For TL, samples were heated from 25 to 325 °C with a heating rate of 5 °C s^{-1} under nitrogen flow. Background was not subtracted. Each luminescence measurement process was repeated for three samples under the same conditions. The maximum measurement uncertainty was ±9%.

3. Results and discussion

3.1. X-ray diffractometry analysis

The x-ray diffraction patterns of pure (undoped) BAlMgLi and samples doped with cerium concentrations (BAlMgLi:xCe), with x between 0.1 and 0.5%, are shown in Fig. 1.

Fig. 1 shows the x-ray diffraction pattern of BAlMgLi glass samples, pure and doped with xCe, where x = 0.1, 0.2, 0.3, 0.4, and 0.5%. The x-ray diffractograms do not show sharp or discrete peaks but do display a broad amorphous halo (band) centered at approximately 22° (2θ) and a smooth halo at approximately 45° (2θ) in the pure sample, and in doped samples with 0.2, 0.3, 0.4, and 0.5% of cerium. These results indicate the absence of atomic arrangements of long-range order and therefore shows the amorphous/glassy nature (Meera and Ramakrishna, 1993; Kaur et al., 2012). In the diffractogram of the sample with 0.1% Ce, the broad halo at about 40° (2θ) and a weak peak at about 72° (2θ) were observed; the peak is attributed to CeO_2 (Joint Committee on Powder

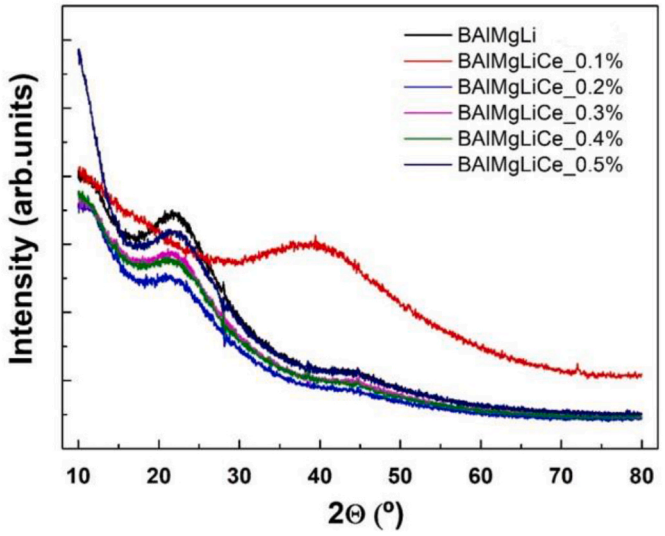

Fig. 1. X-ray diffractograms of pure and Ce-doped BAlMgLi.

Diffraction Standards - JCPDS, number 251164). Since the intensity of this peak is low, it can be assumed that the CeO_2 content does not affect the structural properties of the material. The temperature variations experienced by the sample may have contributed to the appearance of the peak. All diffractograms show a small band around 38° (2θ), which is attributed to Al_2O_3 according to the Inorganic Crystal Structure Database (ICSD) 92631.

3.2. Vibrational analysis

3.2.1. Raman vibrational spectroscopy

Fig. 2 shows the Raman spectra of the pure and cerium-doped samples maintained at 30 °C. The three regions analyzed were from 200 to 900 cm^{-1} (I), 901 to 1500 cm^{-1} (II), and 1501 to 3500 cm^{-1} (III).

In region I, a band at 810 cm^{-1} is observed, which is characteristic of the formation of the boroxol ring, normally identified in Raman spectra of pure borate glasses (Colthup et al., 1990; Maniu et al., 2003). This result implies that boron, in this structure as a network former, did not undergo changes in atomic positions due to the presence of the other constituent elements of the material.

Region II shows two bands. The band at 1235 cm^{-1} is due to the formation of pyroborate, which occurs when one atom of boron is bonded to three of oxygen, and this triangular configuration is bonded to another identical configuration (Li et al., 2001), which makes the glass less hygroscopic. Another band at 1456 cm^{-1} indicates the presence of stretching vibrations of the B–O bond in isolated BO_4 and/or Al–O or Al–O–B units in the aluminum lattice in a metaborate configuration (Brow et al., 1997; Santos et al., 2009; Kaur et al., 2014).

Six bands are observed in region III. Since borate glasses are hygroscopic, they absorb moisture from the air. During the period between production and analysis (7 day at 20 °C), the samples were protected from ambient light but not from moisture. Since H_2O molecules and those from the hydroxyl group are luminescence activators (Garcia-Guinea et al., 2018), they stimulate energy absorption and subsequent re-emission. The bands in this region can be attributed to the presence of water (Shinozaki et al., 2013), which is absorbed from the environment, and hydroxyl groups, which are formed when the water molecule loses a hydrogen atom due to an increase in temperature.

3.2.2. Fourier transform infrared vibrational spectroscopy (FTIR)

The FTIR spectra shown in Fig. 3 reveal the presence of functional groups present in the structure indicated by absorption bands (indicated by arrows) in the pure and Cerium-doped BAlMgLi samples.

The FTIR analyses were also performed in three regions: between 600 and 800 cm^{-1} (I), 801 and 1200 cm^{-1} (II) and 1201 and 1600 cm^{-1} (III). Storage conditions and time between synthesis and characterization followed the standard used for Raman analysis. In region I, a band centered at approximately 704 cm^{-1}, characteristic of borate glasses, explains an atomic bond of type B–O–B in units of BO_3 and BO_4. The increase in the intensity of this band reveals that the entry of cerium is converting BO_3 into BO_4. The band around 806 cm^{-1}, which is due to the boroxol ring, was not identified by this technique, suggesting that the bonds between the atoms are mostly triangular (BO_3) and tetrahedral (BO_4) types. In addition to this band in region I, two other bands were identified at positions 452 cm^{-1} and 550 cm^{-1}; these bands may be due to the presence of CeO_2 groups which affects the BO_3 configuration that affect the BO_3 configuration. This is evident from the observation that there is a slight shift as the amount of Cerio increases (Yadav and Singh, 2012).

Three bands were identified in region II. The band at 850 cm^{-1} is due to aluminum, which contributes to the presence of so-called oxygen bridges, which link two other atomic arrangements in BO_4 (Kaur et al., 2014). The bands at 918 and 1064 cm^{-1} are due to stretching vibrations between the boron and oxygen atoms in a simple configuration (B–O), as well as in a BO_4^- type configuration in triborate, tetraborate, and pentaborate groups (Kaur et al., 2014; Kaur et al., 2012; Singh et al., 2012a). The change in band intensity at 1064 cm^{-1} occurs due to the incorporation of cerium and the consequent change from BO_3 to BO_4 configuration (Yadav and Singh, 2012; Singh et al., 2011).

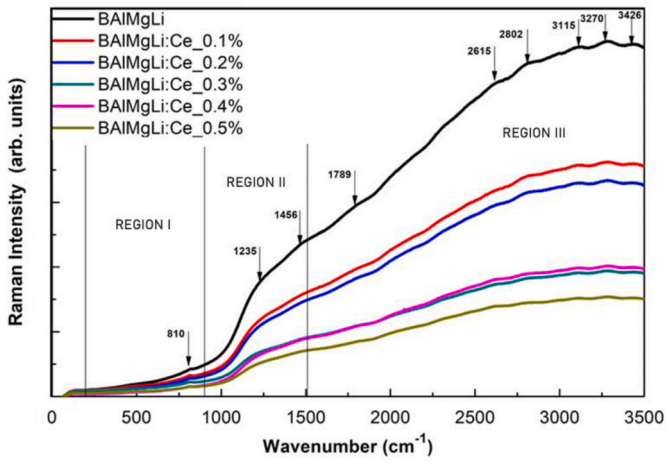

Fig. 2. Raman spectra of pure and Ce-doped BAlMgLi.

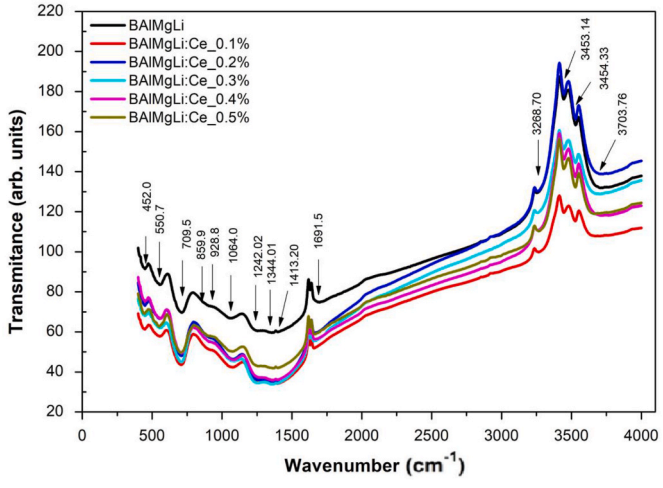

Fig. 3. FTIR of pure and Ce-doped BAlMgLi.

Finally, region III is characterized by a motion associated with the stretching vibrations of the triangular BO_3 units (Souadi et al., 2024; Jabali et al., 2024). The region reveals three bands, two in the interval between 1211 cm^{-1} and 1382 cm^{-1} and another between 1403 cm^{-1} and 1423 cm^{-1}, corresponding to a pronounced asymmetric stretching of the B-O bonds within the BO_3 groups (Souadi et al., 2024; Jabali et al., 2024). These bands are due to stretching vibrations of B–O in BO_3 units in the metaborate, pyroborate, and orthoborate groups (Kaur et al., 2014; Singh et al., 2012b; Valença et al., 2018). The changes in the intensity of the bands in this region are characteristic of competition between the atoms of cerium and aluminum for the occupation of a position in the lattice of the glass; this occurs because of the conversion of BO_3 into BO_4 (Singh et al., 2011; Singh et al., 2012b). Bands above appear in amorphous materials as a characteristic of the presence of hydroxyl groups or water or even B–O–H or O–H bonds (Singh et al., 2012a; Valença et al., 2018). The hydroxyl and water groups are luminescence activators (Garcia-Guinea et al., 2018). The band assignments of the vibrational units in borate glasses are listed in Table 1.

Assignment of the bands of the vibrational units in borate glasses are listed in Table 1.

The incorporation of cerium ions changes the structural configuration of the host matrix, due to the vibration modes of this rare earth element. These can be identified in the IR spectrum of the sintered sample, which presents a vibration band at 1413.20 and 1691.50 cm^{-1} due to Ce ions (Sharma and Dubey, 2023)

3.3. Optically stimulated luminescence

Fig. 4 shows the OSL curves in the form of typical exponentials, with the initial predominance of a rapid decay rate due to direct recombination between electrons and holes in the luminescent centers during optical stimulation (Mckeever and Yukihara, 2008). The glasses doped with 0.3% and 0.5% cerium showed higher intensity in the OSL signal. The non-doped sample showed no OSL signal.

The experimental OSL curves were fitted using the three-component exponential function shown in Equation (1):

$$I_{OSL} = A_1 e^{-t/\tau_1} + A_2 e^{-t/\tau_2} + A_3 e^{-t/\tau_3} \quad (1a)$$

where I_{OSL} is OSL intensity; A_1, A_2, and A_3 are constant coefficients; τ_1, τ_2, and τ_3 are the decay constants related to the types of traps (Valença et al., 2018). Table 2 shows the values of the parameters obtained by adjusting Equation (1) in the OSL curves.

As can be seen, the fast component is predominant in all samples, indicating the occurrence of direct recombination between electrons and holes in the luminescent centers (Mckeever and Yukihara, 2008). The luminescence does not reach zero in the evaluated interval of 40 s, indicating that the process of recapture of the loads occurs in shallow traps before recombination (Valença et al., 2018). Shallow traps are those where there is ease of releasing electrons with low energy stimulus; so, wavelengths in the visible light range are sufficient for electron detrapping. The electrons are recaptured by other shallow traps or traps of greater depth (Nyirenda, 2018; Rivera-Montalvo et al., 2021).

Fig. 5 shows the dependence of the intensity of the OSL signal on the absorbed doses in the range between 2 and 12 Gy. OSL intensities were defined by the area over the emission curves. It is noted that the OSL signal of the samples showed a tendency to increase with the dose in the analyzed interval. The sample doped with 0.5% cerium presented a more intense OSL signal while the pure sample showed no relevant alteration of its signal.

Table 1
Assignments made for the FTIR spectra as illustrated in Fig. 3.

Spectral band position (cm^{-1})	Infrared assignments	Reference
~704	B–O–B atomic bonding in BO_3 and BO_4 units	Kaur et al. (2014)
~806	Presence of the boroxol ring	Kaur et al. (2012), Balachander et al. (2013)
~850	Oxygen bridges	Kaur et al. (2014)
~918 to 1064	Stretching vibrations. Presence of triborate, tetraborate, and pentaborate groups	Kaur et al. (2012), Singh et al. (2012a)
~1064	Configuration change in the structure (BO_3 to BO_4)	Kaur et al. (2014), Singh et al. (2011)
~1211, 1382, 1403, 1423	Stretching vibrations in metaborate, pyroborate, and orthoborate groups	Singh et al. (2012b), Hrúby (1972)

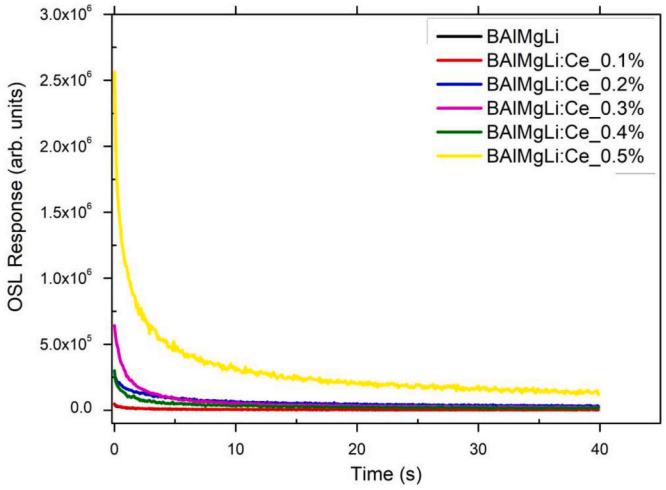

Fig. 4. OSL curves of pure and Ce-doped BAlMgLi irradiated with 2 Gy of $^{90}Sr + ^{90}Y$.

Table 2
Values of the parameters obtained by adjusting Equation (1) in the OSL curves.

Sample	OSL Component	Decay constant τ(s)
BAlMgLi	Fast	0.09 ± 0.01
	Medium	1.46 ± 0.12
	Slow	9.99 ± 1.42
BAlMgLi:Ce (0.1% Ce)	Fast	0.09 ± 0.02
	Medium	0.91 ± 0.07
	Slow	7.30 ± 0.49
BAlMgLi:Ce (0.2% Ce)	Fast	0.51 ± 0.05
	Medium	3.26 ± 0.30
	Slow	19.41 ± 0.47
BAlMgLi:Ce (0.3% Ce)	Fast	0.49 ± 0.47
	Medium	2.29 ± 0.01
	Slow	13.01 ± 1.18
BAlMgLi:Ce (0.4% Ce)	Fast	0.10 ± 0.01
	Medium	1.15 ± 0.05
	Slow	9.79 ± 0.54
BAlMgLi:Ce (0.5% Ce)	Fast	0.49 ± 0.47
	Medium	2.29 ± 0.01
	Slow	13.01 ± 1.18

3.4. Thermoluminescence

TL emissions (Fig. 6) of samples of pure and Ce-doped BAlMgLi show a broad emission peak resulting from the superposition of two peaks. During sample heating, electrons trapped in shallower traps are released faster than electrons trapped in deeper traps (Pagonis et al., 2006), resulting in the shift of the broad emission. Taking into account that the intensity of the TL signal increases as a function of the amount of Ce, it can be concluded that the traps generated by the dopant are shallower. Lanthanide and lithium ions can induce electron traps associated with defects and impurities (Kitagawa et al., 2021). The TL signal of the doped samples is attributed to electronic transitions. of the cerium ion

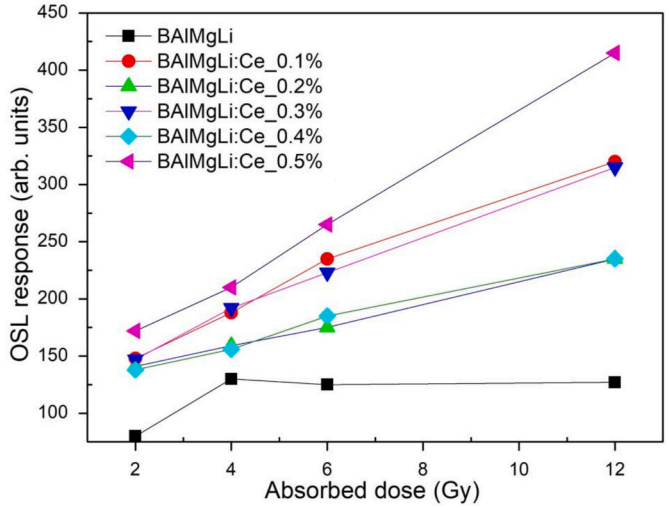

Fig. 5. OSL response of pure and Ce-doped BAlMgLi as a function of absorbed dose from $^{90}Sr + {}^{90}Y$.

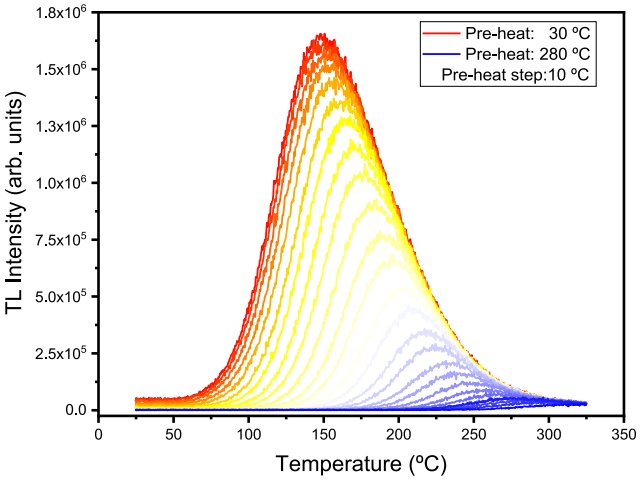

Fig. 7. TL curves of BAlMgLi:Ce (0.3% Ce) after pre-heat process, from 30 °C to 280 °C, with pre-heat step of 10 °C.

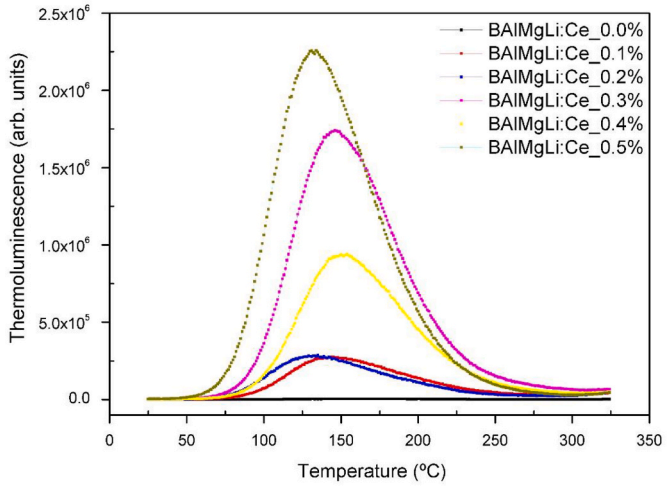

Fig. 6. TL emission of pure and Ce-doped BAlMgLi irradiated with 2 Gy of $^{90}Sr + {}^{90}Y$.

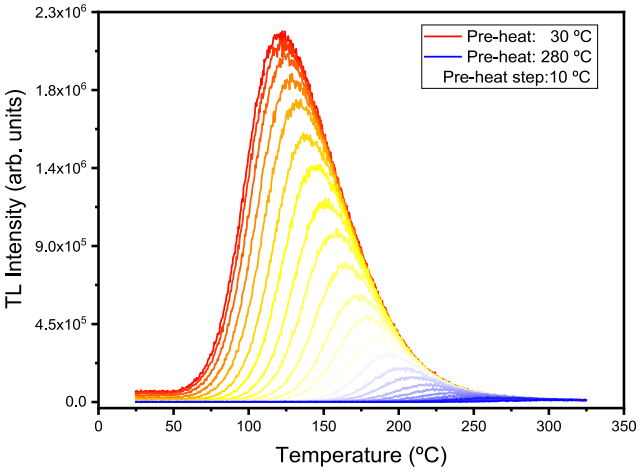

Fig. 8. TL curves of BAlMgLi:Ce (0.5% Ce) after pre-heat process, from 30 °C to 280 °C, with pre-heat step of 10 °C.

(Ce^{3+}) 5 d → 4f (Dorenbos, 2000).

Analyses of TL emissions (Fig. 6) of samples of pure and Ce-doped BAlMgLi show the presence of a broad emission peak in all samples studied, which is the result of the overlapping of two peaks. Lanthanide and lithium ions can induce electron capture centers associated with defects and impurities (Kitagawa et al., 2021). The TL signal of the doped samples is attributed to electronic transitions of the cerium (Ce3+) 5 d → 4f ion (Dorenbos, 2000). The intensity of the TL signal increases as a function of the percentage of the Ce dopant indicating that the traps generated by the dopant are shallow.

When conducting an analysis of the thermoluminescent behavior of magnesium and lithium aluminoborate glasses that have been doped with cerium at concentrations of 0.3% and 0.5%, the repeated initial rise (RIR) method was employed within a stopped temperature range (T_{stop}) of 30 °C to 280 °C, utilizing increments of 10 °C. It was observed that there is a nonlinear response to changes in the concentration of traps (Figs. 7 and 8). This nonlinearity implies that there are multiple luminescence emission processes occurring, which could potentially be linked to various states of energy traps present within the band gap of the material. These states can influence the release of trapped electrons under different thermal conditions, which can be seen through the shifts in the maximum temperature (T_m) during the RIR method (Kitagawa et al., 2022; Pagonis et al., 2018).

Moreover, the phenomenon of the progressive displacement of T_m towards higher values indicates that there is a varying energy density of the traps. This suggests that there may be a continuous distribution of trap states rather than a discrete and well-defined distribution. This behavior becomes even more intriguing when considering the amorphous nature of glasses, where the lack of periodicity in the atomic structure can result in a wider range of intermediate energy levels that electrons can become trapped within (Sadek, 2020; Kumar et al., 2017).

The persistence of this continuous trap distribution behavior, even with variations in the concentration of the dopant cerium, strongly suggests that the distribution of traps is correlated with the overall structure of the doped material. This correlation could potentially be linked to the topology of the band gap and the distribution of the trap sites. These findings highlight the necessity for a more comprehensive investigation into the atomic structure and characteristics of the trap sites within these glasses in order to gain a deeper understanding of the observed thermoluminescent dynamics (Sadek, 2020; Kumar et al., 2019).

The repeated RIR method eliminates the need to calculate the frequency factor s, regardless of the peak order in the TL glow curve.

Equation (1) allowed for a linear fit of ln(I) values from TL curves pre-heated between 80 °C and 260 °C, yielding the activation energies for 0.3% Ce and 0.5% Ce doped samples.

$$\ln(I(T)) = c - \frac{E}{k_b T} \quad (1b)$$

where I(T) is the TL Intensity, T is temperature in kelvin, E is activation energy in eV, kb is Boltzmann constant (eV/K), and c is an arbitrary constant. Fig. 9 shows the plot of the activation energies.

Table 3 shows the activation energy values of the trap levels as well as the average energy for the respective sets. The association of BAlMgLi: Ce trap levels (0.3% Ce and 0.5% Ce) with similar energies, in the form of sets (A, B and C), can help to describe the behavior of a distribution continuum of energy sublevels.

The activation energies were defined only for the temperature range up to 180 °C, because at higher temperatures the uncertainties of the RIR method are high due to the reduced residual intensity of the TL emission curve.

To investigate the linearity of the TL signal response to absorbed dose, samples were irradiated with increasing doses between 0.09 Gy and 2.72 Gy (Fig. 10). The TL signal values were obtained by integrating the area under the emission curve.

The dose-response curves showed a tendency towards a linear relationship between the intensity of the TL response and the dose in the range studied, which is an indication of good dosimetric performance of a material (Bos, 2001; Azorin, 2014). Linear fitting revealed a range of response linearity in the dose range studied, with linear correlation coefficients of 0.999 for undoped samples; for doped samples, these were 0.996 for 0.1% Ce samples, 0.2% Ce, 0.994 for 0.3% Ce, 0.985 for 0.4% Ce, and 0.899 for 0.5% Ce.

To evaluate the reproducibility of the luminescent signal of the samples, five cycles of irradiation (2 Gy) – reading – heat treatment were performed. This process was repeated five times, and the results are illustrated in Fig. 11. The average value of the percentage coefficient of variation of TL intensities was 7.46%. This result meets the requirements that are disseminated by the International Organization for Standardization, (ISO, 2000), which states that this coefficient should not exceed 10%, in order to ensure appropriate reproducibility of the luminescent signal of the studied samples.

Fig. 12 shows the OSL fading for the first instants of samples irradiated with 2 Gy. On the x-axis, "delay" means the time elapsed between the irradiation and the reading of the OSL signal. The fading is intense,

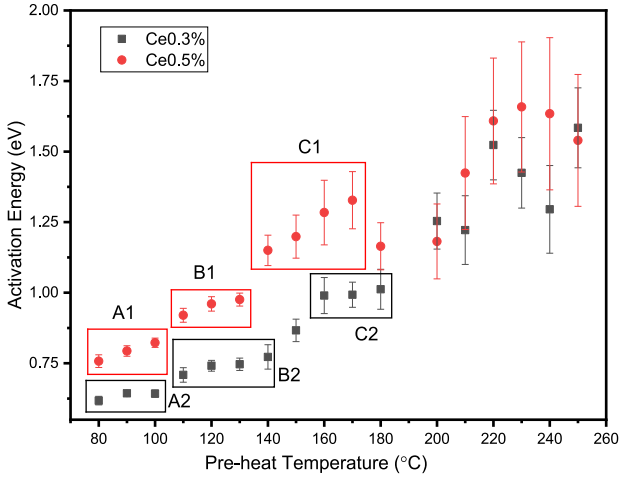

Fig. 9. Activation Energies for 0.3% Ce and 0.5% Ce samples. The inner rectangles named by A1, A2, B1, B2, C1, and C2 represent trap levels with a similar activation energy.

Table 3
Mean Activation Energy for the A, B and C regions.

Samples	Mean Activation Energy (eV)		
	A	B	C
0.3% Ce	0.634 ± 0.012	0.732 ± 0.022	0.905 ± 0.048
0.5% Ce	0.791 ± 0.019	1.002 ± 0.032	1.259 ± 0.010

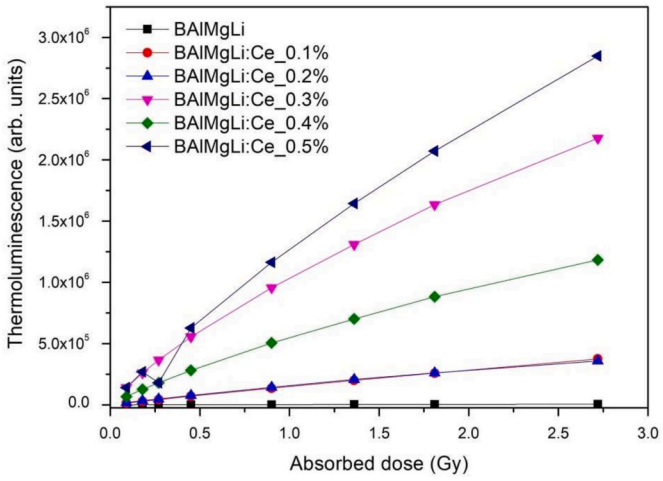

Fig. 10. TL intensity of pure and Ce-doped BAlMgLi as a function of absorbed dose.

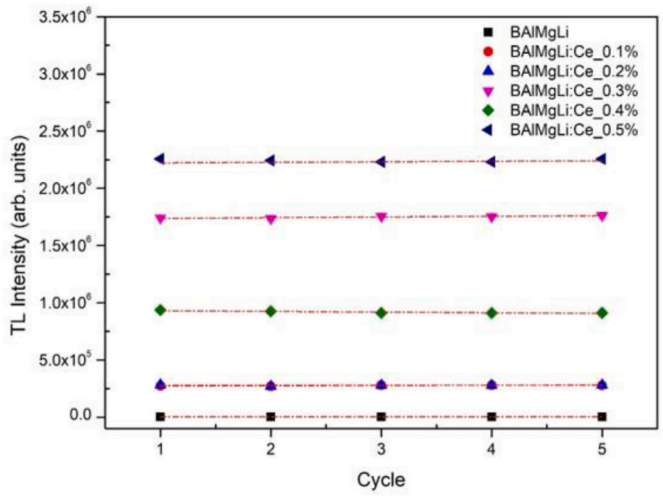

Fig. 11. Reproducibility of the luminescent signal of the pure and Ce-doped BAlMgLi irradiated with 2 Gy.

reaching 90% of the thermoluminescent signal after almost 70 days of irradiation. This behavior corroborates the indication that the traps generated by the Ce dopant are shallow. The intensities were normalized by a common factor.

The interest in new glasses with applications in TL and OSL dosimetry has remained. For example, Elkholy (2010) studied the thermoluminescence characteristics of lithium borate glasses and their dependence on different MgO concentrations. Although the study involved doses in the order of kGy, the emission curve is similar to that our material, with a single peak, but at a higher temperature. This type of emission curve with a broad peak is expected in borate glass. (Hashim et al., 2014; Efenji et al., 2023). In a more recent study, cerium-doped barium borate glasses were prepared by Środa et al. (2019) in the BaO-B2O3 system and investigated by TL and OSL. The TL response of

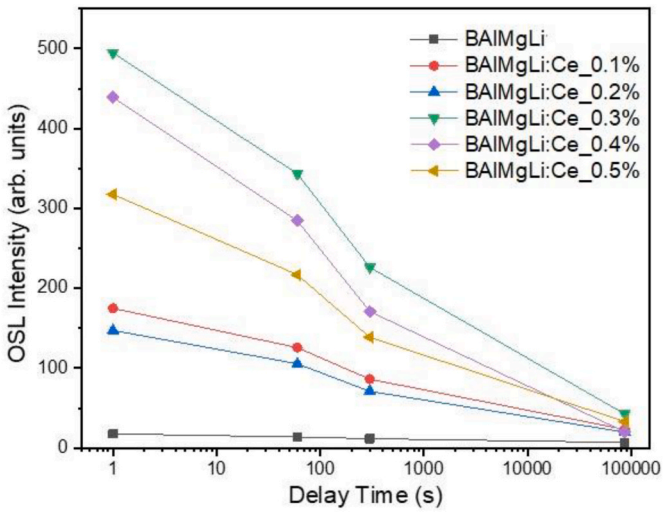

Fig. 12. Fading of the luminescent signal of the pure and Ce-doped BAlMgLi irradiated with 2 Gy.

the material was proportional to the radiation dose in the range of 2–10 Gy, but we could note that, in contrast to the Ce-doped BAlMgLi samples, the results showed a predominance of a slow decay of the OSL signal. In another study, Tb^{3+} ions doped sodium magnesium aluminum borosilicate glasses were recently investigated by Li et al. (2024), who concluded that the new materials have potential as for blue-green lasers and dosimetry.

4. Conclusion

Pure BAlMgLi and doped BAlMgLi:xCe samples present diffractograms characteristic of vitreous materials. The Raman and FTIR spectra of the samples showed the presence of a boroxol ring, which indicates that boron is the main network former.

The OSL signals of the samples presented curves with an exponential decay. In the range analyzed, the response to the radiation dose in the TL and OSL analyses was dependent on the dopant concentration. The samples doped with 0.3% and 0.5% cerium showed the highest response in the analyzed dosage range.

Therefore, the insights obtained through the utilization of the RIR method offer valuable perspectives on the intricate relationship between the atomic structure, trap distribution, and luminescent behavior of these materials. A thorough understanding of these aspects not only holds implications for the manipulation of their luminescent properties for specific applications, but also presents opportunities for the development of new materials that possess optimized properties for use in sensors, optical devices, and related fields.

The charge recapture process occurs in shallow traps before charge recombination. In the range analyzed, the response to the radiation dose was dependent on the dopant concentration for all samples. Perhaps due to the disordered nature of the glass structure, the traps form a continuous set of energy levels.

From the spectroscopic and luminescent analyzes carried out, it is possible to infer that the new glass matrix studied in this work is not very hygroscopic, has a reproducible luminescent signal, and can be exploited for different applications.

CRediT authorship contribution statement

Allan W.S. Santos: Writing – original draft, Methodology, Formal analysis, Conceptualization. **Iury S. Silveira:** Writing – review & editing, Investigation. **Luiz C. Meira-Belo:** Investigation. **Andrea L.F. Novais:** Writing – review & editing, Investigation. **Divanizia N. Souza:** Writing – review & editing, Supervision, Resources, Formal analysis.

Declaration of competing interest

The authors declare the following financial interests/personal relationships which may be considered as potential competing interests: Divanizia do Nascimento Souza reports equipment, drugs, or supplies was provided by Federal University of Sergipe. If there are other authors, they declare that they have no known competing financial interests or personal relationships that could have appeared to influence the work reported in this paper.

Acknowledgments

The authors thank the Brazilian agencies Comissão Nacional de Energia Nuclear (CNEN), Coordenação de Aperfeiçoamento de Pessoal de Nível Superior - CAPES and Conselho Nacional de Desenvolvimento Científico e Tecnológico - CNPq (Projects: 307008/2022–3, 407493/2021–2, 406761/2022–1 - National Institute of Radiation Technology in Health Science (INTERAS)

Data availability

Data will be made available on request.

References

Alajerami, Y.S.M., Hashim, S., Ramli, A.T., Saleh, M.A., Kadni, T., 2013. Thermoluminescence properties of Li2CO3–K2CO3–H3BO3 glass system co-doped with CuO and MgO. Radiat. Protect. Dosim. 155, 1–10.

Ardiansyah, A., Heryanto, H., Armynah, B., Salah, H., Sulieman, A., Bradley, D.A., Tahir, D., 2023. Physical, mechanical, optical, and gamma radiation shielding properties of the BaO-based glass system prepared by the melt-quench technique: a review. Radiat. Phys. Chem. 210, 111059.

Azorin, J., 2014. Preparation methods of thermoluminescent materials for dosimetric applications. An overview. Appl. Radiat. Isot. 83, 187–191.

Balachander, L., Ramadevudu, G., Shareefuddin, M., Sayanna, R., Venudhar, Y., 2013. IR analysis of borate glasses containing three alkali oxides. Sci. Asia 39 (3), 278.

Barrera, G.R., Souza, L.F., Novais, A.L.F., Caldas, L.V.E., Abreu, C.M., Machado, R., et al., 2019. Thermoluminescence and optically stimulated luminescence of PbO–H3BO3 and PbO–H3BO3–Al2O3 glasses. Radiat. Phys. Chem. 155, 150–157.

Bos, A.J.J., 2001. High sensitivity thermoluminescence dosimetry. Nucl. Instrum. Methods Phys. Res. B 184 (1–2), 3–28. https://doi.org/10.1016/S0168-583X(01)00717-0.

Brow, R.K., Tallant, D.R., Turner, G.L., 1997. Polyhedral arrangements in lanthanum aluminoborate glasses. J. Am. Soc. 80, 1239–1244.

Colthup, N.B., Daly, L.H., Wiberley, S.E., 1990. Introduction to Infrared and Raman Spectroscopy, 3rd. Academic Press Inc. ISBN 0-12-182554-X.

Daisuke, N., Go, O., Yutaka, F., Naoki, K., Noriaki, K., Takayuki, Y., 2017. Optical and radiation-induced luminescence properties of Ce-doped magnesium aluminoborate glasses. Opt. Mater. 72, 190–194.

Del Sol Fernández, S., García-Salcedo, R., Guzmán, Mendoza J., Sánchez-Guzmán, D., Ramírez-Rodríguez, G., Gaona, E., Rivera-Montalvo, T., 2016. Thermoluminescent characteristics of LiF:Mg,Cu,P and $CaSO_4$:Dy for low dose measurement. Appl. Radiat. Isot. 111, 50–55. https://doi.org/10.1016/j.apradiso.2016.02.011.

Dogan, T., Yüksel, M., Akça, S., Portakal, Z.G., Balci-Yegen, S., Kucuk, N., Topaksu, M., 2017. Normal and anomalous heating rate effects on thermoluminescence of Ce-doped ZnB2O4. Appl. Radiat. Isot. 128 (2017), 256–262. https://doi.org/10.1016/j.apradiso.2017.07.032.

Dorenbos, P., 2000. The 5d level positions of the trivalent lanthanides in inorganic compounds. J. Lumin. 91, 155–176.

Efenji, G.I., et al., 2023. Description and dosimetric features of lithium borate glass doped with transition metals for thermoluminesce, a re-evaluation. Phys. Scripta 98 (5), 052001.

El-Adawy, A., Khaled, N.E., El-Sersy, A.R., Hussein, A., Donya, H., 2010. TL dosimetric properties of Li2O–B2O3 glasses for gamma dosimetry. Appl. Radiat. Isot. v. 68, 1132–1136.

Elkholy, M.M., 2010. Thermoluminescence of B_2O_3–Li_2O glass system doped with MgO. J. Lumin. 130, 1880–1892. https://doi.org/10.1016/j.jlumin.2010.05.002.

Feller, S.A., Hannon, A.C., Wright, A.C. (Eds.), 1997. Borate Glasses, Crystal & Melts. Society of glass technology.

Garcia-Guinea, J., Correcher, V., Can, N., Garrido, F., Townsend, P.D., 2018. Cathodoluminescence spectra recorded from surfaces of solids with hydrous molecules. J. Electron. Spectrosc. Relat. Phenom. https://doi.org/10.1016/j.elspec.2018.05.008.

Hashim, S., Alajerami, Y.S.M., Ramli, A.T., Ghoshal, S.K., Saleh, M.A., Kadir, A.A., et al., 2014. Thermoluminescence dosimetry properties and kinetic parameters of lithium

potassium borate glass co-doped with titanium and magnesium oxides. Appl. Radiat. Isot. 91, 126–130.
Hrúby, A., 1972. Evaluation of Glass-forming tendexy by means of DTA. J. Phys. 22, 1187–1193.
Huang, W., Wen, Z., Li, L., Ashraf, G.A., Chen, L., Lei, L., et al., 2022. Photoluminescence and X-ray excited scintillating properties of Tb3+-doped borosilicate aluminate glass scintillators. Ceram. Int. 48 (12), 17178–17184. https://doi.org/10.1016/j.ceramint.2022.02.274.
Iordanova, R., Mancheva, M., Dimitriev, Y., Klissurski, D., Tyuliev, G., Kunev, B., 2009. Synthesis of $ZrMo_2O_8$ polymorphs by a melt quenching method and mechanochemical activation. J. Alloys comp. 485 (1–2), 104–109. https://doi.org/10.1016/j.jallcom.2009.06.064.
ISO, E., 2000. 9001: 2000. Quality management systems-Requirements (ISO 9001: 2000).
Jabali, D.A., Madkhli, A.Y., Souadi, G., Ümit, H.K., Coban, M.B., Madkhali, O., Ayvacikli, M., Nasser, Amri, Can, N., 2024. Temperature-responsive insights: investigating Eu^{3+} and Dy^{3+} activated yttrium calcium oxyborate phosphors for structure and luminescence. Appl. Radiat. Isot. 206, 111214.
Kaur, P., Singh, G.P., Kaur, S., 2012. Modifier role of cerium in lithium aluminium borate glasses. J. Mol. Struct. 1020, 83–87. https://doi.org/10.1016/j.molstruc.2012.03.053.
Kaur, S., Singh, G.P., Kaur, P., Singh, D.P., 2013. Cerium luminescence in borate glass and effect of aluminium on blue green emission of cerium ions. J. Lumin. 143, 31–37.
Kaur, P., Kaur, S., Singh, G.P., Singh, D.P., 2014. Cerium and samarium codoped lithium aluminoborate glasses for white light emitting devices. J. Alloys Compd. 588, 394–398.
Kaur, R., Rakesh, R.B., Mhatre, S.G., Bhatia, V., Kumar, D., Singh, H., et al., 2021. Structural and optical properties of Ce3+ doped borosilicate doped glasses. J. Mater. Sci. Mater. Electron. 32, 18381–18396.
Kawano, N., Kawaguchi, N., Okada, G., Fujimoto, Y., Yanagida, T., 2018. Scintillation and dosimetric properties of Ce-doped strontium aluminoborate glasses. J. Non-Crystal. Sol. 482, 154–159. https://doi.org/10.1016/j.jnoncrysol.2017.12.030.
Kitagawa, Y., Yukihara, E.G., Tanabe, S., 2021. Development of Ce^{3+} and Li co-doped magnesium borate glass ceramics for optically stimulated luminescence dosimetry. J. Lumin. 232, 117847.
Kitagawa, Y., Jumpei, U., Setsuhisa, T., 2022. Blue persistent phosphor of YSiO2N:Ce3+ developed by codoping Sm3+ or Tm3+ ions and thermoluminescence analysis of their trap distributions. Phys. Status Solidi 219 (5), 2100670, 2022.
Kucuk, N., Kucuk, I., Yüksel, M., Topaksu, M., 2016. Thermoluminescence characteristics of Zn (BO2) 2: Ce3+ under beta irradiation. Radiat. Protect. Dosim. 168 (4), 450–458.
Kumar, D., Rao, S.M., Singh, S.P., 2017. Structural, optical and thermoluminescence study of Dy3+ ion doped sodium strontium borate glass. J. Non-crystal. Solids 464, 51–55.
Kumar, D., Rao, S.M., Singh, S.P., 2019. Effect of Er^{3+} on NaSrB glass: thermoluminescence and structural analysis. Appl. Phys. 125, 1–10. https://doi.org/10.1007/s00339-018-2319-5.
León-Alfaro, M.A., Morales-Hernández, A., Roman-Lopez, J., Zarate-Medina, J., Rivera-Montalvo, T., 2018. Optically and thermally stimulated luminescence characteristics of LaAlO3:Pr3+ beta irradiated. Appl. Radiat. Isot. 132, 57–60. https://doi.org/10.1016/j.apradiso.2017.11.020.
Li, Y., Dong, Z., Xu, S., Wu, C., Chen, J., Zhang, C., Mahadevan, C.K., 2024. Photoluminescence and thermoluminescence performance in Tb^{3+}-activated aluminum borosilicate glass with high thermal stability for blue-green laser and TLD applications. Ceram. Int. 50 (20), 38445. https://doi.org/10.1016/j.ceramint.2024.07.209.
Li, H., Su, Y., Li, L., Strachan, D.M., 2001. Raman spectroscopic study of gadolinium (III) in sodium-aluminoborosilicate glasses. J. Non-Cryst. Solids 292, 167–176. https://doi.org/10.1016/S0022-3093(01)00878-X.
López-Esquivel, R.I., Guzmán-Olguín, J.C., Vázquez-Flores, N., Correcher, V., Benavente, J.F., Guzmán-Mendoza, J., Montalvo, T.R., 2023. Green syntesis, structural and luminescent characterization of BaZrO3:Eu3+ nanoparticles. Ceram. Int. 49, 413–418. https://doi.org/10.1016/j.ceramint.2022.09.004.
Maniu, D., Iliescu, T., Ardelean, I., Cinta-Pinzaru, S., Tarcea, N., Kiefer, W., 2003. Raman study on B2O3–CaO glasses. J. Mol. Struct. 651, 485–488. https://doi.org/10.1016/S0022-2860(03)00129-7.
Mckeever, S.W.S., Yukihara, E.G., 2008. Optically stimulated luminescence (OSL) dosimetry in medicine. Phys. Med. Biol. 53. https://doi.org/10.1088/0031-9155/53/20/R01.
Meera, B.N., Ramakrishna, J., 1993. Raman spectral studies of borate glasses. J. Non-Cryst. Solids 159, 1–21. https://doi.org/10.1016/0022-3093(93)91277-A.
Mohan, S., Kaur, S., Singh, D.P., Kaur, P., 2017. Structural and luminescence properties of samarium doped lead alumino borate glasses. Opt. Mater. 73, 223–233. https://doi.org/10.1016/j.optmat.2017.08.015.
Nakauchi, D., Okada, G., Fujimoto, Y., Kawano, N., Kawaguchi, N., Yanagida, T., 2017. Optical and radiation-induced luminescence properties of Ce-doped magnesium aluminoborate glasses. Opt. Mater. 72, 190–194.
Nyirenda, N., 2018. Combined Spectral and Stimulated Luminescence Study of Charge Trapping and Recombination Processes in α-Al_2O_3:C. Phd. Thesis. Faculty of Science Rhodes University.
Oglakci, M., Topaksu, M., Can, N., 2020. Thermoluminescence glow curves of beta irradiated NaBaBO3: Ce3+ phosphor synthesized by combustion method. Sensor Actuator Phys. 315, 112299.
Oglakci, M., Portakal-Uçar, Z.G., Akça-Özalp, S., Correcher, V., Benavente, J.F., Sonsuz, M., Can, N., Halefoglu, Y.Z., Topaksu, M., 2023. Thermoluminescence behavior of Ce3+ doped lanthanum tri-borate phosphor for dosimetry applications. Ceram. Int. 49 (22), 36092–36102.
Omar, R.S., Hashim, S., Bradley, D.A., Karim, M.K.A., Kobayashi, I., Kadir, A.B.A., Hashim, A., 2022. Al2O3: C and LiF: Mg, Ti characterisations at 100–150 kV energy range for computed tomography dose measurement. Radiat. Phys. Chem. 199, 110365.
Pagonis, V., Kitis, G., Furetta, C., 2006. Numerical and Practical Exercises in Thermoluminescence, first ed. ed. Springer, New York.
Pagonis, V., Santos Vieira, F.M., Chambers, A., Anthony, L., 2018. Thermoluminescence glow curves in preheated feldspar: a Monte Carlo study. Nucl. Instr. Meth.in Phys. B. 436, 249–256.
Rittisut, W., Wantana, N., Ruangtaweep, Y., Rujirawat, S., Kidkhunthod, P., Manyum, P., et al., 2022. New developments in the Gd3+/Sm3+ ions doped lithium aluminum borate glasses of luminescent materials for lighting applications. Radiat. Phys. Chem. 201, 110443. https://doi.org/10.1016/j.radphyschem.2022.110443.
Rivera-Montalvo, T., Alvarez-Romero, R., Morales-Hernandez, A., Zarate-Medina, J., 2021. Luminescence characteristics of perovskite type LaAlO3:Dy3+ for radiation detector. J. Lumin. 240, 118403. https://doi.org/10.1016/j.jlumin.2021.118403.
Sadek, A.M., 2020. Revealing the theoretical assumptions of the trap-depth distribution model in the thermoluminescence theory. Thin Solid Films 714, 138390.
Sadeq, M.S., Abdo, M.A., 2021. Effect of iron oxide on the structural and optical properties of alumino-borate glasses. Ceram. Int. 47 (2), 2043–2049. https://doi.org/10.1016/j.ceramint.2020.09.036.
Santiago, M., Santiago, M., Lavat, A., Caselli, E., Caselli, E., Lester, M., et al., 1998. Thermoluminescence of strontium tetraborate. Phys. Status Solidi 167, 233–236.
Santos, C.N., Sousa Meneses, D., Echegut, P., Neuville, D.R., Hernandes, A.C., Ibanez, A., 2009. Structural, dielectric, and optical properties of yttrium calcium borate glasses. Appl. Phys. Lett. 94, 8–10.
Sharma, S., Dubey, S.K., 2023. Enhanced luminescence studies of synthesized $Ca_2MgSi_2O_7$: Ce^{3+} phosphor. COJ Biom. Science Research 2 (3), 000538.
Shinozaki, H., Nakashima, S., Takahashi, S., Hanada, A., Yamamoto, Y., 2013. Water resistance of cerium phosphate glasses as studied by in situ high temperature IR microspectroscopy. J. Non-crystal. Solids 378, 55–60.
Singh, G.P., Kaur, P., Kaur, S., Singh, D.P., 2011. Role of WO_3 in structural and optical properties of WO3–Al2O3–PbO–B2O3 glasses. Cond. Matter 406, 4652–4656. https://doi.org/10.1016/j.physb.2011.09.052.
Singh, G.P., Kaur, S., Kaur, P., Singh, D.P., 2012a. Modification in structural and optical properties of ZnO, CeO_2 doped Al_2O_3-PbO-B_2O_3 glasses. Cond. Matter 407, 1250–1255. https://doi.org/10.1016/j.physb.2012.01.114.
Singh, G.P., Kaur, P., Kaur, S., Singh, D.P., 2012b. Investigation of structural, physical and optical properties of CeO2-Bi2O3-B2O3 glasses. Physica B: Cond. Metter 407, 4168–4172. https://doi.org/10.1016/j.physb.2012.06.043.
Souadi, G., Nasser, A., Ümit, H.K., Coban, M.B., Madkhali, O., Ayvacikli, M., Can, N., 2024. Novel Sm^{3+} doped $YCa_4O(BO_3)_3$ phosphors: structural and, low and room temperature luminescent insights. Appl. Radiat. Isot. 203, 111114.
Souza, L.F., Nolasco, A., Barrera, G.R., Campos, W.R.C., Souza, D.N., Nogueira, M.S., 2021. Evaluation of MgB4O7: Ce, Li and Ce-doped 80MgB2O4–20MgB4O7 as alternative OSL materials for use in quality assurance of 6 MV photon beams. Radiat. Phys. Chem. 182, 109355.
Środa, M., Świontek, S., Gieszczyk, W., Bilski, P., 2019. The effect of CeO2 on the thermal stability, structure and thermoluminescence and optically stimulated luminescence properties of barium borate glass. J. Non-Cryst. Solid. 517, 61–69. https://doi.org/10.1016/j.jnoncrysol.2019.03.026.
Ugalde-Valdés, M.A., Nolasco-Altamirano, D., López-Ruiz, L.E., Guzmán-Mendoza, J., Rivera-Montalvo, T., 2023. TL glow curve and kinetic analysis of Na2SiO3:Pr3+ under beta radiation effect. Appl. Radiat. Isot. 198, 110850. https://doi.org/10.1016/j.apradiso.2023.110850.
Valença, J.V., Silva, A.C., Dantas, N.O., Caldas, L.V., d'Errico, F., Souza, S.O., 2018. Optically stimulated luminescence of the $20Li_2CO_3$ – (X)K_2CO_3– (80 - X) B_2O_3 glass system. J. Lumin. 200, 248–253. https://doi.org/10.1016/j.jlumin.2018.03.060.
Vogel, W., 1994. Glass Chemistry, 2nd. Springer-Verlag, New York.
Yadav, A.K., Singh, P.A., 2012. Modifier Role of Cerium in Glasses by Raman Spectroscopy. Royal Society of Chemistry. *Varanasi*-221005 (India).
Yahaba, T., Fujimoto, Y., Yanagida, T., Koshimizu, M., Tanaka, H., Saeki, K., Asai, K., 2017. Thermoluminescence and optically stimulated luminescence properties of Dy3+-doped CaO–Al2O3–B2O3-based glasses. Nucl. Instrum. Methods Phys. Res. B 392, 36–40. https://doi.org/10.1016/j.nimb.2016.12.011.
Zubair, H.T., Begum, M., Moradi, F., Rahman, A.M., Mahdiraji, G.A., Oresegun, A., et al., 2020. Recent advances in silica glass optical fiber for dosimetry applications. IEEE Photon. J. 12 (3), 1–25.